

Neuronal cell type–specific alternative splicing is regulated by the KH domain protein SLM1

Takatoshi Iijima, Yoko Iijima, Harald Witte, and Peter Scheiffele

Biozentrum, University of Basel, 4056 Basel, Switzerland

The unique functional properties and molecular identity of neuronal cell populations rely on cell type–specific gene expression programs. Alternative splicing represents a powerful mechanism for expanding the capacity of genomes to generate molecular diversity. Neuronal cells exhibit particularly extensive alternative splicing regulation. We report a highly selective expression of the KH domain–containing splicing regulators

SLM1 and SLM2 in the mouse brain. Conditional ablation of SLM1 resulted in a severe defect in the neuronal isoform content of the polymorphic synaptic receptors neurexin-1, -2, and -3. Thus, cell type–specific expression of SLM1 provides a mechanism for shaping the molecular repertoires of synaptic adhesion molecules in neuronal populations *in vivo*.

Introduction

Understanding the molecular mechanisms that direct the differentiation and connectivity of neuronal cells in the brain remains one of the major challenges in cell biology (Shen and Scheiffele, 2010; Zipursky and Sanes, 2010). Neuronal cell types are characterized by unique morphological and functional properties that shape signal processing in neuronal networks (Masland, 2004; Okaty et al., 2011). The remarkable diversity of neuronal properties is achieved by cell type–specific gene expression programs. Alternative splicing greatly amplifies the coding capacity of the genome and, thereby, provides a powerful mechanism controlling molecular and functional diversity. For example, alternative splicing programs control abundance, identity, transport, and turnover of certain neuronal mRNAs (Darnell, 2013; Zheng and Black, 2013). Ultimately, these RNA regulatory mechanisms contribute to the control of selective cell surface interactions, ion channel properties, and neuronal signaling (Siddiqui et al., 2010; Beck et al., 2012; Gehman et al., 2012; Lipscombe et al., 2013). It is an attractive hypothesis that cell type–specific alternative splicing factors are used to shape the molecular repertoires of

functionally and morphologically defined sub-classes of neuronal cells. However, splicing factors that are linked to a genetically defined subsets of neurons and that are essential to sculpt cell type–specific neuronal gene expression are only beginning to emerge.

The KH domain–containing RNA-binding protein SAM68 (Src-associated in mitosis of 68 kD protein, *Khdrbs1*) is a critical regulator of RNA transport and neuronal activity–regulated alternative splicing (Iijima et al., 2011; Klein et al., 2013). SAM68 is broadly expressed in neuronal and nonneuronal cells and regulates alternative splicing of *Nrxn1*, which encodes a synaptic cell surface receptor (Missler and Südhof, 1998; Dean et al., 2003; Craig and Kang, 2007; Südhof, 2008; Iijima et al., 2011). Cerebellar *Sam68^{KO}* neurons fail to increase exon skipping at the *Nrxn1* alternatively spliced segment 4 (AS4) upon neuronal depolarization. In wild-type neurons, this SAM68-dependent exon skipping results in production of NRX protein variants with altered ligand interactions (Boucard et al., 2005; Chih et al., 2006; Graf et al., 2006; Uemura et al., 2010; Iijima et al., 2011; Matsuda and Yuzaki, 2011; Aoto et al., 2013). Consistent with an important function for SAM68 *in vivo*, there is a corresponding reduction in the skipped AS4(–) transcript in *Sam68^{KO}* brains. Global ablation of the closely related RNA-binding protein SLM2 (SAM68-like mammalian protein 2; alternate names: T-STAR, *Khdrbs3*; Di Fruscio et al., 1999;

Correspondence to Peter Scheiffele: peter.scheiffele@unibas.ch

T. Iijima's present address is Tokai University, Institute of Innovative Science and Technology, Medical Science Division, Shimokasuya 143, Isahara City, Kanagawa 259-1193, Japan.

Abbreviations used in this paper: AS4, alternatively spliced segment 4; CCK, cholecystokinin; nPTBP, neural poly-pyrimidine tract binding protein; NRX, neurexin protein; *Nrxn*, Neurexin gene; PPA, perforant path–associated; SAM68, Src-associated in mitosis of 68-kD protein; SCA, Schaffer collateral associated; SLM, SAM68-like mammalian protein; S.L.M., *stratum lacunosum moleculare*; S.O., *stratum oriens*; S.R., *stratum radiatum*; VIP, vasoactive intestinal peptide.

© 2014 Iijima et al. This article is distributed under the terms of an Attribution–Noncommercial–Share Alike–No Mirror Sites license for the first six months after the publication date (see <http://www.rupress.org/terms>). After six months it is available under a Creative Commons License (Attribution–Noncommercial–Share Alike 3.0 Unported license, as described at <http://creativecommons.org/licenses/by-nc-sa/3.0/>).

Supplemental Material can be found at:
<http://jcb.rupress.org/content/suppl/2014/01/22/jcb.201310136.DC1.html>

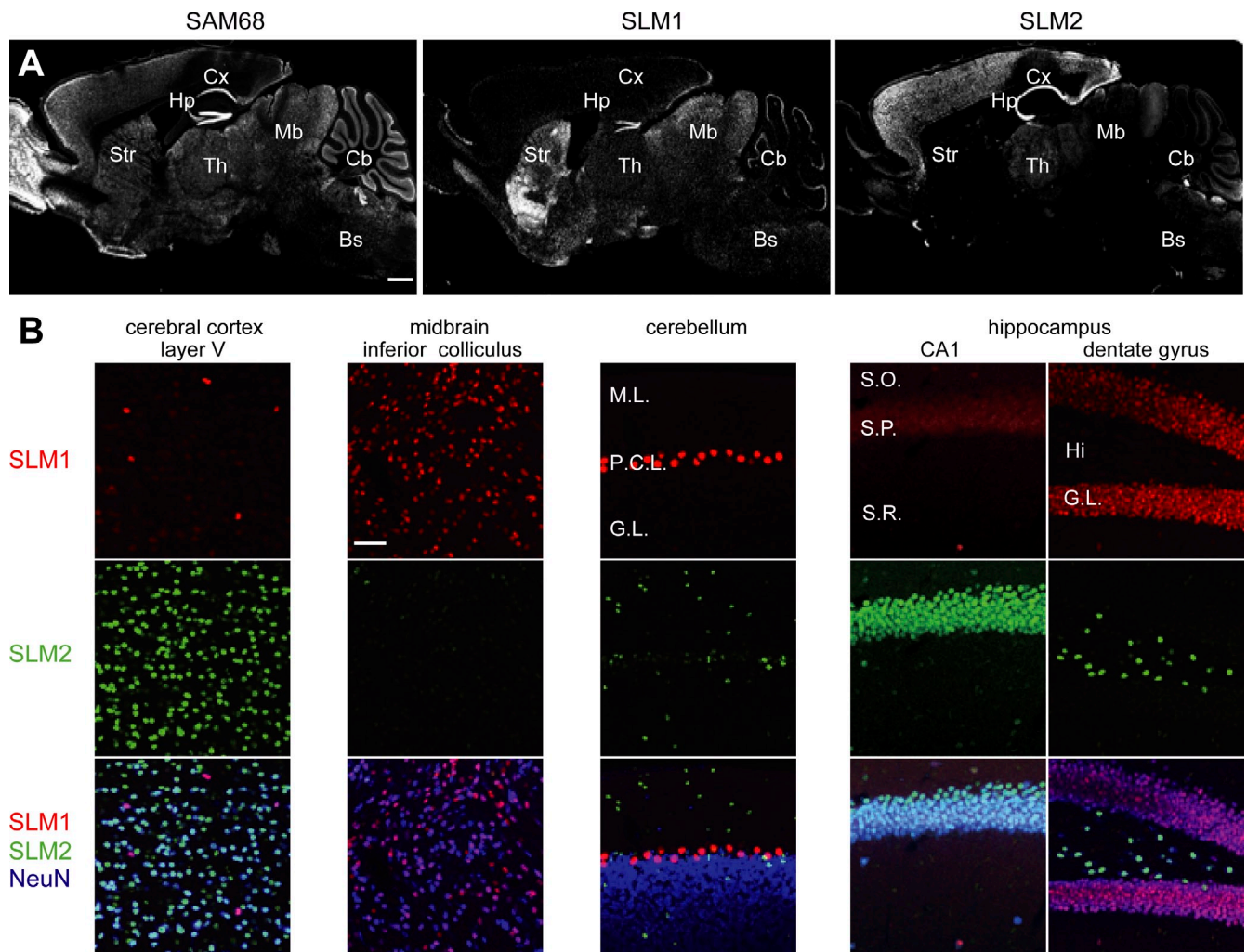


Figure 1. **Differential distribution of SLM1 and SLM2 proteins in the mouse brain.** (A) Gross expression patterns of STAR family proteins in adult brain. Cx, cortex; Hp, hippocampus; Str, striatum; Th, thalamus; Mb, midbrain; Cb, cerebellum; Bs, brain stem. Bar, 1 mm. (B) High magnification images of SLM expression in various brain areas. I–III, cortical layer I–III; M.L., molecular layer; P.C.L., Purkinje cell layer; G.L., granular layer. S.O., *stratum oriens*; S.P., *stratum pyramidale*; S.R., *stratum radiatum*. Hi, hilus. Bar, 50 μ m.

Venables et al., 1999) also results in a reduction in exon skipping at *Nrxn* AS4, which correlates with the regional expression levels of SLM2 in the brain (Ehrmann et al., 2013). These studies established SAM68 and SLM2 in alternative splicing regulation in the mouse brain. However, it is not known whether the activity of these proteins is essential to generate cell type-specific gene expression programs in defined neuronal cell populations.

In this work, we uncover that SLM2 and the closely related SLM1 are expressed in highly selective and largely nonoverlapping populations of neurons in the central nervous system of mice. In the hippocampus, SLM1 is abundant in glutamatergic dentate granule cells but also in a specific set of cholecystokinin–calbindin double-positive (CCK⁺ calbindin⁺) inhibitory interneurons. By contrast, SLM2 is confined to glutamatergic pyramidal cells and GABAergic parvalbumin⁺, calretinin⁺, and somatostatin⁺ interneurons. We demonstrate that SLM1 differs from SAM68 in its ability to regulate alternative splicing of different *Nrxn* mRNAs at AS4 in vitro. *Slm1*^{KO} mice and *Sam68:Slm1*^{DKO} exhibit a severe

reduction in *Nrxn1* AS4(–) transcripts as well as defects in cerebellar morphogenesis. Finally, we demonstrate that cell type-specific conditional ablation of SLM1 disrupts cell type-specific generation of *Nrxn* splice variants. Thus, SLM1 is a critical RNA-binding protein that shapes cell type-specific alternative splicing programs in vivo.

Results

SLM1 and SLM2 are expressed in largely segregated neuronal populations

Western blotting analysis of different mouse brain areas with SAM68, SLM1, and SLM2 antibodies indicates that these proteins are detectable across all brain regions examined (Fig. S1A). To explore whether SLM proteins are confined to specific anatomically and molecularly defined neuronal populations, we performed a detailed analysis using SLM1- and SLM2-specific antibodies. SLM1 and SLM2 were detected in largely nonoverlapping cell populations, whereas SAM68 is more widely expressed (Fig. 1A; Fig. S1, B and C). In the cortex, SLM1 marks

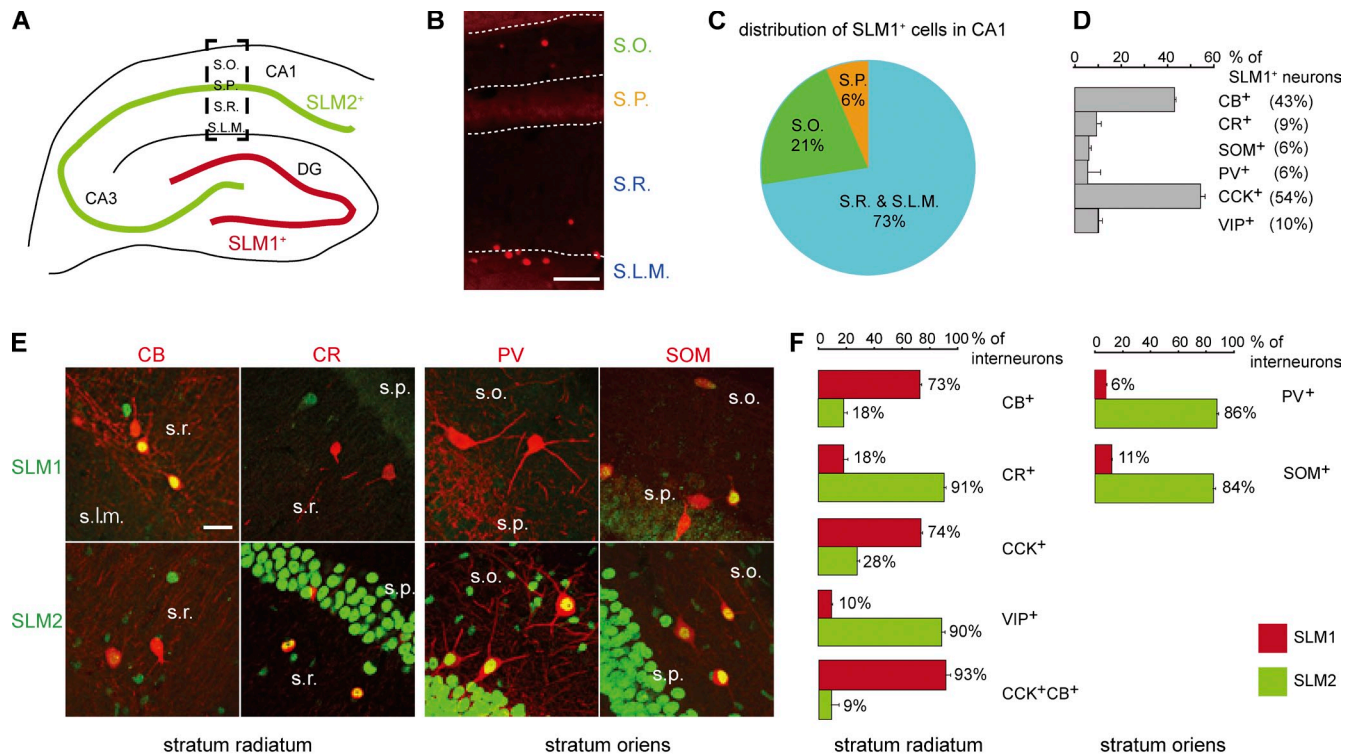


Figure 2. Hippocampal interneuron subclass-specific expression of SLM1 and SLM2. (A) Schematic illustration of expression of SLM proteins in principal cells of the hippocampal area. (B) SLM1-positive interneurons in hippocampal area CA1. Bar, 100 μ m. S.R., *stratum radiatum*; S.L.M., *stratum lacunosum moleculare*; S.P., *stratum pyramidale*; S.O., *stratum oriens*. (C) Distribution of SLM1-positive interneurons in CA1. The percentage of SLM1+ cells that are located in each stratum was quantified. (D) Percentage of SLM1-positive interneurons that are immuno-positive for various inhibitory interneuron markers within *stratum radiatum* and *stratum lacunosum moleculare* of CA1 (right; $n = 3$ animals). (E) Mutually exclusive expression of SLM1 and SLM2 in hippocampal interneurons immuno-positive for calbindin (CB), calretinin (CR), parvalbumin (PV), and somatostatin (SOM). Coronal sections (from 2–3-mo-old mice) were co-immunostained with anti-SLM antibodies and inhibitory interneuron markers. Bar, 20 μ m. (F) Fraction of SLM1- and SLM2-positive cells within immunohistochemically defined inhibitory interneuron populations in area CA1 ($n = 3$ animals).

a sparse population of cells in layers 2–3 and layer 5, whereas SLM2 is expressed in the majority of NeuN-positive cortical cells (Fig. 1 B; unpublished data). By contrast, SLM2 is largely absent from midbrain neurons of the *superior* and *inferior colliculus* where the majority of cells express SLM1 (Fig. 1 B). In the cerebellum, SLM1 is highly concentrated in Purkinje cells, whereas SLM2 marks interneurons in the inner granular and molecular layer. Thus, SLM1 and SLM2 are restricted to subpopulations of neurons in the mouse brain.

A particularly interesting segregation of SLM1 and -2 is seen in the mature hippocampus. In principal cells, SLM2 is detectable exclusively in CA neurons, whereas SLM1 is highly expressed in dentate granule cells (Fig. 1 B; Fig. S2 A; Stoss et al., 2004). Notably, both proteins are also highly expressed in nonoverlapping populations of inhibitory interneurons (Fig. S2 B). SLM2 is concentrated in interneurons in the hilus (Fig. 1 B, dentate gyrus; Fig. S2 A). Within area CA1, the majority of SLM1-positive (SLM1⁺) cells are located in *stratum radiatum* (S.R.) and its border to the *stratum lacunosum moleculare* (S.L.M.; Fig. 2, A–C). We applied a combination of interneuron markers to directly define this population. 43% of all SLM1⁺ cells were marked with the interneuron marker calbindin and 54% were immuno-positive for CCK (Fig. 2 D). Conversely, \sim 70% of all calbindin⁺ and 70% of all CCK⁺ interneurons in S.R. and S.L.M. expressed

SLM1 (Fig. 2, E and F). SLM1 was largely absent from calretinin⁺, vasoactive intestinal peptide (VIP)⁺, parvalbumin⁺, and somatostatin⁺ interneurons. Calbindin and CCK immunoreactivity overlap in two specific interneuron populations in S.R./S.L.M. designated Schaffer collateral-associated (SCA) interneurons and perforant path-associated (PPA) interneurons (Lawrence, 2008; Klausberger, 2009). Interestingly, 93% of these CCK/calbindin double-positive interneurons showed SLM1 immunoreactivity. These results identify SCA interneurons and PPA interneurons as a major site of SLM1 expression (Fig. 2 F; Fig. S2 C). Calbindin and CCK-positive interneurons largely lack detectable SLM2 immunoreactivity, which instead was observed in the vast majority (>90%) of calretinin and VIP-positive interneurons in S.R. and S.L.M. Moreover, in *stratum oriens* (S.O.) SLM2 was highly expressed in parvalbumin⁺ and somatostatin⁺ interneurons (Fig. 2, E and F). These experiments uncover a striking non-overlapping distribution of SLM1 and SLM2 in vivo. The quantitative analysis with cell type-specific markers demonstrates that the respective SLM1- and SLM2-positive cell populations are not due to stochastic expression or detection of the proteins in subsets of cells. By contrast, expression is tightly linked to molecularly defined cell identity. Thus, SLM1 and -2 are well suited to regulate neuronal alternative splicing programs in a cell type-specific manner.

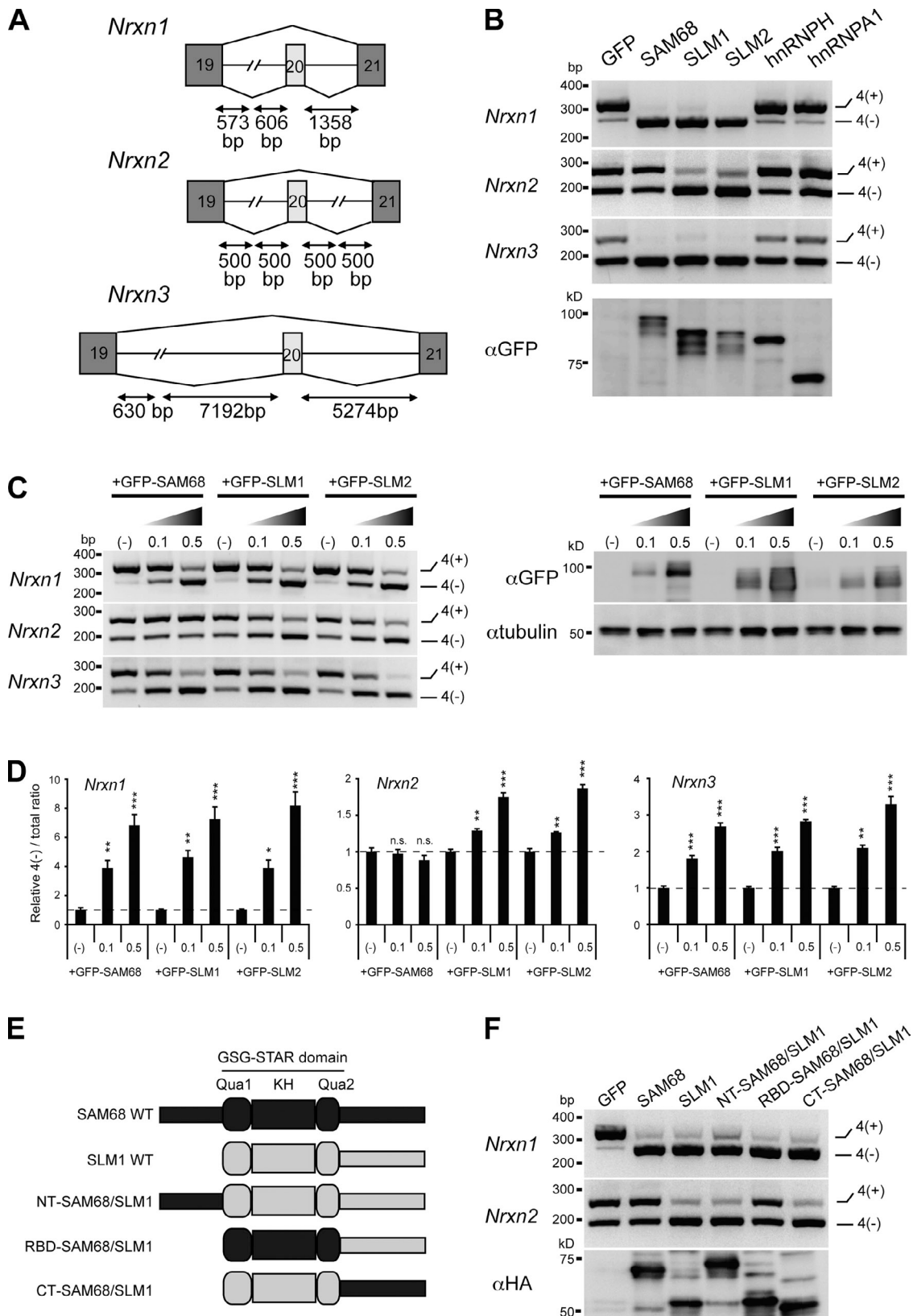


Figure 3. Function of SLM proteins in *Nrxn1*, *Nrxn2*, and *Nrxn3* alternative splicing regulation in vitro. (A) Splice reporters for *Nrxn1*, *Nrxn2*, and *Nrxn3* AS4. *Nrxn* splice reporter constructs contain AS4 with constitutive exons (dark gray), alternative exon 20 (light gray), and introns shown as lines. Intron sizes are indicated (drawings not to scale). (B) Splice reporter assays with various RNA-binding proteins. Reporter expression vectors were cotransfected into HEK293T cells with epitope-tagged expression constructs for GFP-SAM68, GFP-SLM1, GFP-SLM2, YFP-hnRNP A1, or YFP-hnRNP H1. Alternative splice isoform choice was measured by semi-quantitative RT-PCR with primers flanking the alternatively spliced segment. Fragment sizes for AS4(+) and AS4(-) isoforms are 318 bp and 228 bp (*Nrxn1*), 270 bp and 180 bp (*Nrxn2*), and 354 bp and 264 bp (*Nrxn3*). Expression of transfected RNA-binding proteins

SLM1 regulates *Nrxn2* alternative splice reporters in heterologous cells

In previous work we demonstrated that SAM68, SLM1, and SLM2 can regulate *Nrxn1* splice reporters (“mini-genes”) when transfected into human embryonic kidney cells (HEK293; Iijima et al., 2011). Given the highly selective expression of SLM1, we asked whether its ability to regulate mRNA targets might differ from SAM68. When SAM68, SLM1, and SLM2 activity toward *Nrxn1*, *Nrxn2*, and *Nrxn3* splice reporters was analyzed in HEK293 cells we observed that all three proteins could efficiently drive exon skipping at *Nrxn1* and *Nrxn3* AS4. Importantly, SAM68 did not exhibit significant activity toward a *Nrxn2* AS4 reporter, whereas SLM1 and SLM2 did induce exon skipping in *Nrxn2* (Fig. 3, A and B). Under the same conditions, hnRNPH and A1 did not show activity toward any of the *Nrxn* AS4 reporters (Fig. 3 B). The specific activity of SLM proteins toward *Nrxn2* reporters was further confirmed in assays with increasing amounts of the alternative splicing factors (Fig. 3, C and D).

To obtain insight into the molecular underpinnings of the target specificity of SAM68 versus SLM1 we generated chimeric forms of these RNA-binding proteins (Fig. 3 E). SAM68 differs from SLM1 and SLM2 in an extended N-terminal region of 96 amino acids that is absent in the SLM proteins. Fusion of this N-terminal domain to SLM1 did not alter its ability to regulate *Nrxn2*, indicating that this domain is not sufficient to abolish alternative splicing regulation toward *Nrxn2* (Fig. 3 F). Replacement of the SLM1 RNA-binding domain with corresponding sequences from SAM68 rendered this protein inactive toward *Nrxn2*. By contrast, replacement of the C-terminal domain with SAM68 sequences did not modify activity toward *Nrxn2*. Importantly, all chimeric proteins retained activity toward processing of the *Nrxn1* reporter, thereby confirming appropriate folding and subcellular targeting of the chimeric proteins (Fig. 3 F). These experiments demonstrate that SLM1 differs from SAM68 in that it exhibits activity toward *Nrxn2* and that this activity arises from specific sequences in the SLM1 RNA-binding domain.

Co-expression and complex formation of SLM1 and SAM68

Whereas SLM1 and SLM2 expression are largely segregated at the cellular level, SLM1 and SAM68 are coexpressed in individual cells (note that given the broad distribution of SAM68 also most SLM2-positive cells co-express SAM68; Fig. 4 A; Fig. 1 A; unpublished data). Previous in vitro studies demonstrated that SLM1 and SAM68 form protein complexes that are not detected for SLM2 (Di Fruscio et al., 1999; Rajan et al., 2009). We confirmed SAM68–SLM1 association in co-immunoprecipitation experiments from transfected HEK293 cells

(Fig. 4 B). To further explore complex formation in brain tissue we performed coimmunoprecipitation experiments for the endogenous proteins and observed robust, RNA-independent association between SAM68 and SLM1 but not SLM2 (Fig. 4 C). Given that STAR proteins are thought to function as oligomers that bind to bi-partite RNA motifs (Galarneau and Richard, 2009; Meyer et al., 2010), we examined whether SAM68–SLM1 complex formation would alter activity toward *Nrxn2*. Co-expression of increasing amounts of SAM68 progressively inhibited the activity of SLM1 toward *Nrxn2* AS4 without modifying the activity toward *Nrxn1* (Fig. 4 D). In the same assay, SAM68 was much less potent in inhibiting SLM2 activity toward *Nrxn2* (Fig. 4 D), consistent with a preferential complex formation between SAM68 and SLM1. Thus, substrate specificity of STAR family proteins can be modulated by hetero-oligomer formation.

Anatomical alterations in *Slm1*^{KO} and *Sam68:Slm1*^{DKO} mice

To explore functions of SLM1 in vivo we generated a conditional *Slm1* allele in mice. Exon 2 of the *Khdrbs2* gene (which encodes SLM1) was flanked by loxP sites (Fig. S3 A). Global *Slm1*^{KO} mice were subsequently generated by Cre-mediated recombination in the germline. Homozygous *Slm1*^{KO} mice completely lacked SLM1 protein expression but did not show detectable alterations in SAM68 or SLM2 expression levels (Fig. 5, A–C). Knockout animals were born at Mendelian frequencies, were viable and fertile, and did not exhibit any obvious behavioral alterations (Fig. 5 D). An anatomical survey of adult *Slm1*^{KO} brains did not reveal any gross anatomical defects (Fig. 5 A). Given that SAM68 and SLM1 have overlapping substrates and are largely coexpressed in neuronal populations, we further generated *Sam68:Slm1* double-knockout mice (*Sam68:Slm1*^{DKO}). These animals were viable but not fertile (consistent with the previously reported function for SAM68 in reproduction). We did not detect major alterations in the distribution of synaptic markers in the hippocampus or cerebellum of the double-knockout mice (Fig. S3, B and C). However, *Sam68:Slm1*^{DKO} mice had slightly smaller brains than wild-type animals and cerebella of *Slm1*^{KO} and *Sam68:Slm1*^{DKO} were significantly reduced in weight (Fig. 5 E). Interestingly, the cerebella of *Sam68:Slm1*^{DKO} exhibited a defect in foliation with loss of the cerebellar fissure separating lobules VIb and VII (Fig. 5 F, phenotype observed in four out of four *Sam68:Slm1*^{DKO} animals but none of their single-knockout littermates or wild-type controls). This defect was not observed in either single-knockout model, although the depth of the fissure was slightly reduced in *Sam68*^{KO} mice (Fig. 5 G). These findings demonstrate a redundant function of *Slm1* and *Sam68* in cerebellar morphogenesis. Within the fused region of lobules VIb and VII the Purkinje cell layer was disorganized, with ectopic Purkinje cells scattered in

was confirmed by Western blotting with anti-GFP antibodies. (C) Dose-dependent activity of STAR family proteins toward *Nrxn1*, *Nrxn2*, and *Nrxn3* AS4. Splice reporter processing was assessed in experiments with increasing amounts of DNA encoding RNA-binding proteins transfected (DNA amounts used indicated in micrograms). (D) Alternative splicing was assayed by semi-quantitative RT-PCR. Expression levels of GFP-tagged proteins were detected by immunoblot. (E) Schematic drawing of domain organization of SAM68 and SLM1 and chimeric mutant proteins. An HA-tag was attached to the C-terminal end of each open reading frame. (F) Splice reporter assays with chimeric proteins using *Nrxn1* and *Nrxn2* AS4 reporters. Alternative splicing was assayed by semi-quantitative RT-PCR. Expression of the HA-tagged proteins was confirmed by immunoblotting.

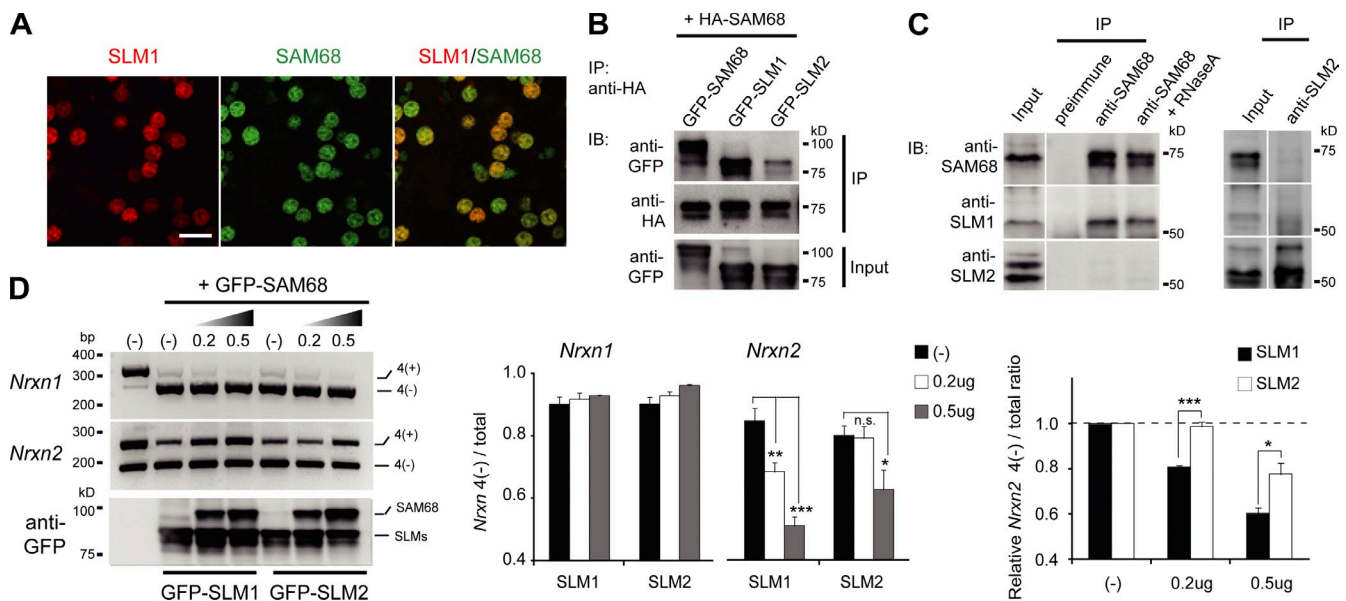


Figure 4. Different regulation of STAR proteins in alternative splicing regulation in vitro. (A) Co-expression of SAM68 and SLM1 in vivo. SAM68 and SLM1 proteins are detected coexpressed in a subset of midbrain neurons in the adult mouse brain. Bar, 20 μ m. (B) Co-immunoprecipitation of HA-tagged SAM68 and GFP-tagged SAM68, SLM1, or SLM2 from HEK293 cells cotransfected with expression constructs. Immunoprecipitation was performed with the anti-HA antibody and proteins in input or immunoprecipitates were detected with anti-HA or anti-GFP antibodies. (C) Complex formation of SAM68 and SLM1 in brain extracts. Complexes were precipitated with either anti-SAM68 (left) or anti-SLM2 (right) antibodies and precipitates probed with anti-SAM68, anti-SLM1, or anti-SLM2 antibodies. When indicated, lysates were treated with Ribonuclease A before antibody addition to eliminate interactions that depend on integrity of cellular RNAs. (D) Alternative splicing of *Nrxn1* and *Nrxn2* AS4 was assayed by semi-quantitative RT-PCR. To confirm protein expression levels, the lysates of HEK293 cells expressing GFP-SLM1 or GFP-SLM2 and increasing amounts of GFP-SAM68 and were subjected to the immunoblotting. Quantitation of alternative splice isoform choice is displayed on the right.

the molecular layer (Fig. 5 H). SLM1 is highly expressed in Purkinje cells. Thus, the foliation phenotype most likely originates from a specific developmental deficit in this cell population.

Cooperation of SAM68 and SLM1 in alternative splicing regulation in vivo

Considering the overlapping functions of SAM68 and SLM1 in the alternative splicing regulation of *Nrxn1* and in cerebellar morphogenesis, we explored whether alternative splicing was modified in *Slm1^{KO}* and *Sam68:Slm1^{DKO}* mice. In *Slm1^{KO}* brains, we detected a 70% reduction of the *Nrxn1* AS4(-) isoforms in midbrain, an area with particularly broad SLM1 expression (Fig. 6, A and B). In the cortex, where only a small sub-population of neurons are SLM1-positive, no significant global change in *Nrxn1* AS4(-) abundance was detected (Fig. 6, B and C). Notably, in the midbrain of *Sam68:Slm1^{DKO}* mice exon skipping at AS4 was severely reduced, demonstrating that SAM68 and SLM1 have synergistic functions in *Nrxn1* alternative splicing regulation in vivo. By contrast, *Nrxn2* alternative splicing at AS4 was not altered in the midbrain of *Sam68^{KO}* mice but selectively disrupted in *Slm1^{KO}* mice (Fig. 6, B and C), consistent with the differential activity of SAM68 and SLM1 toward *Nrxn2* observed in our cellular assays. Finally, we explored alternative splicing at *Nrxn3* AS4 in the midbrain of single- and double-knockout mice. In *Slm1^{KO}* brains skipping of the alternative exon at AS4 was significantly reduced, consistent with a critical function for SLM1 protein in suppressing incorporation of this alternative exon. By contrast, *Sam68^{KO}* mice exhibit a substantial increase in *Nrxn3* AS4 skipping, which was suppressed in

the *Sam68:Slm1^{DKO}* mice. This functional antagonism between SAM68 and SLM1 in vivo was surprising, as both proteins show similar activity toward a *Nrxn3* AS4 reporter in heterologous cells (Fig. 3). Thus, our *Sam68:Slm1^{DKO}* analysis reveals an unanticipated gene-specific interplay of SAM68 and SLM1 functions in the alternative splicing regulation of *Nrxn3*.

Cell type-specific disruption of *Nrxn* alternative splicing

The SLM1 expression pattern suggests that SLM1 may regulate cell type-specific alternative splicing programs. We hypothesized that presence of SLM1 in a neuronal cell population might instruct *Nrxn1* isoform choice. To test this, we mis-expressed SLM1 in cultured cerebellar cells, a largely homogeneous population of granule cells that lacks detectable SLM1 expression and shows predominant expression of *Nrxn* AS4(+) isoforms. Introduction of SLM1 into granule cells was sufficient to stimulate exon skipping and up-regulation of AS4(-) isoforms in *Nrxn1,2,3* (Fig. 7 A). Thus, in this cellular context, SLM1 is sufficient to drive formation of AS4(-) isoforms.

Although the global *Slm1^{KO}* analysis is consistent with a requirement for SLM1 in AS4(-) isoform choice in vivo, this analysis does not allow for conclusions about cell-autonomous function that dictates the molecular repertoire of a defined cell population. To address this issue, we generated conditional knockout mice (*Slm1^{CKO}*) where SLM1 is ablated in Purkinje cells (*Slm1^{fllox/fllox}::Pcp2^{cre}*; Fig. 7 B; Fig. S4). Note that SLM1 remains expressed in a subset of Purkinje cells, in particular in the caudal cerebellum, consistent with the heterogeneity

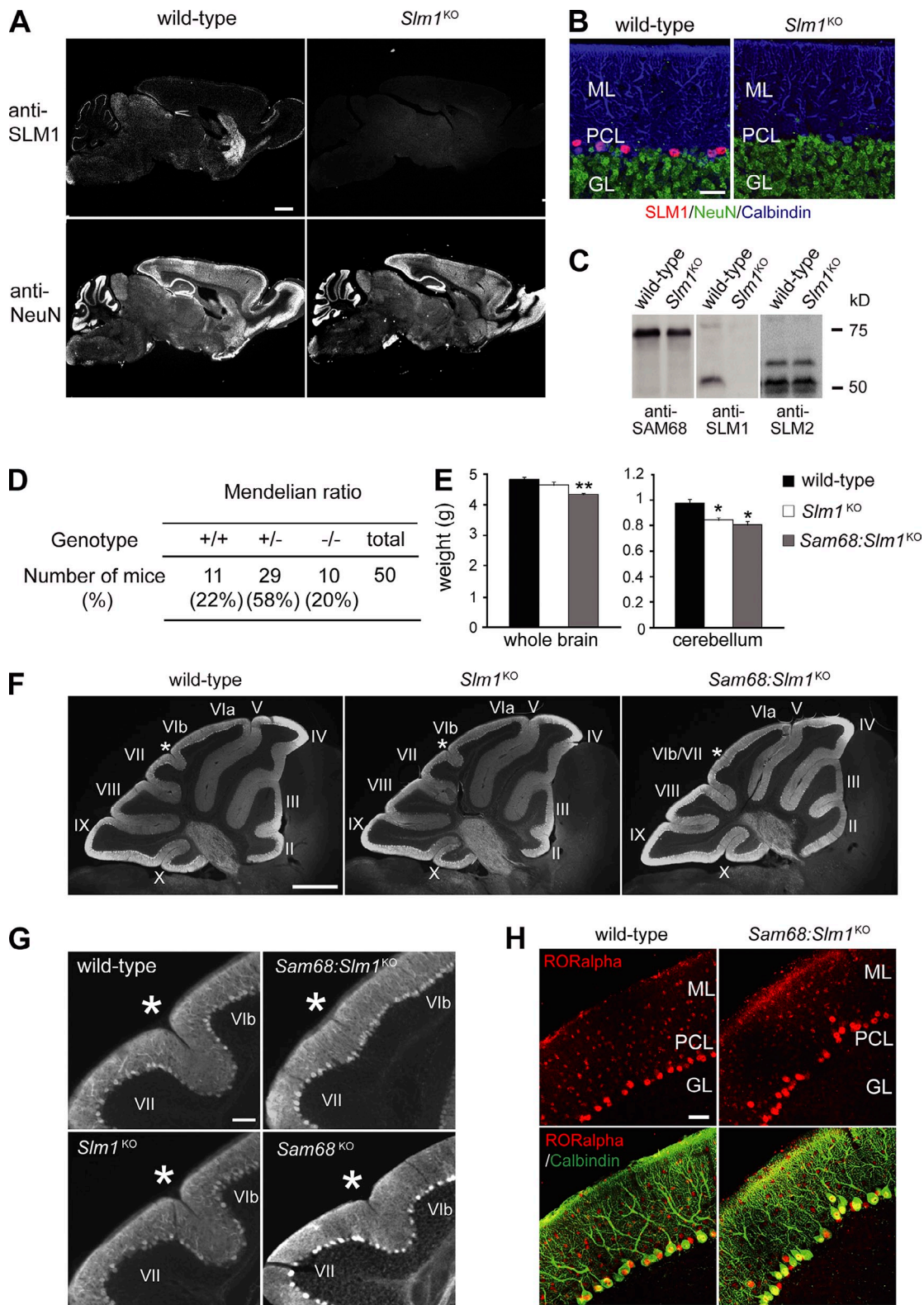


Figure 5. Generation of *Slm1*^{KO} and *Sam68:Slm1*^{DKO} mice. (A) Immunohistochemistry on para-sagittal sections reveals loss of SLM1 immunoreactivity in *Slm1*^{KO} tissue. Bar, 1 mm. (B) High magnification images of immunohistochemistry with anti-SLM1 (red), anti-NeuN (green), and anti-calbindin (blue) antibodies shows loss of SLM1 immunoreactivity from cerebellar Purkinje cells. Bar, 50 μ m. (C) Immunoblot analysis for SAM68, SLM1, and SLM2 in total brain lysates demonstrates loss of anti-SLM1 immunoreactivity in *Slm1*^{KO} tissue. (D) *Slm1*^{KO} mice are born at Mendelian frequencies (50 pups from 4 litters). (E) Weight of whole brains and cerebella from wild-type, *Slm1*^{KO}, and *Sam68:Slm1*^{DKO}. Brain tissues from adult animals were analyzed ($n = 3-4$ animals per genotype). (F) Cerebellar foliation defect of *Sam68:Slm1*^{DKO}. Para-sagittal sections of cerebellar vermis from wild-type, *Slm1*^{KO}, and *Sam68:Slm1*^{DKO} were stained with anti-calbindin antibody to visualize cerebellar foliation. Bar, 1 mm. (G) High magnification images of fissure between lobule VIb and lobule VII in F. Bar, 100 μ m. (H) Co-immunohistochemistry with anti-RORalpha (red) and anti-calbindin (green) antibodies in cerebellar lobule VI revealed abnormal alignment of cerebellar Purkinje cell bodies. Bar, 50 μ m.

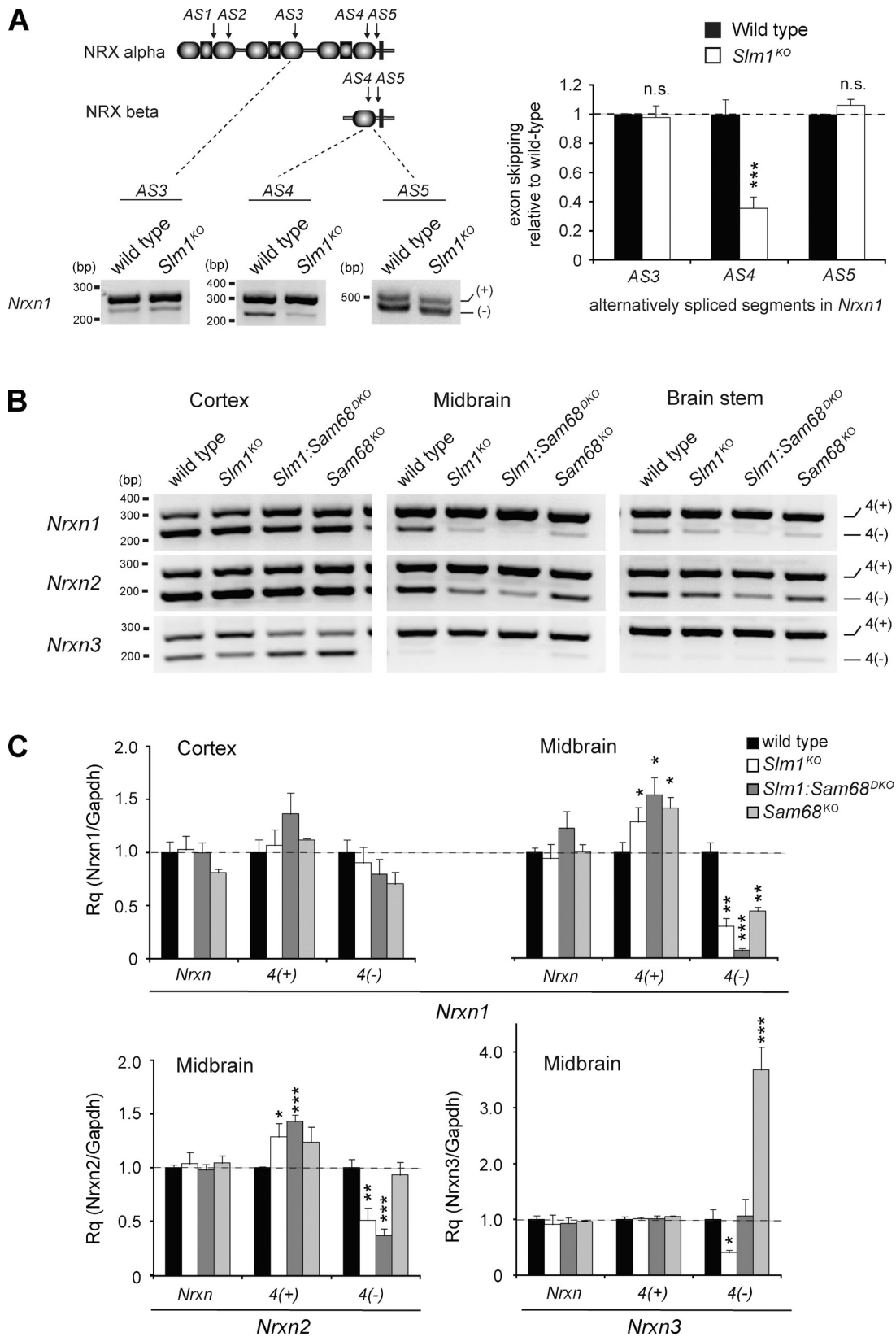


Figure 6. **Alternative splicing defects in *SLM1*^{KO} mice.** (A) Incorporation of alternative exons at AS3, -4, and -5 in midbrain cDNA samples was probed by semi-quantitative PCR with primers flanking the insertion site and analyzed by gel electrophoresis. (B) Representative images of semi-quantitative RT-PCR with *Nrxn* AS4 performed on cortex, midbrain, and brainstem from wild-type, *Slm1*^{KO}, *Sam68:Slm1*^{DKO}, and *Sam68*^{KO} mice. (C) Quantitative RT-PCR performed on cortex and midbrain cDNA samples from wild-type, *Slm1*^{KO}, *Sam68:Slm1*^{DKO}, and *Sam68*^{KO} mice (*n* = 3 animals per genotype).

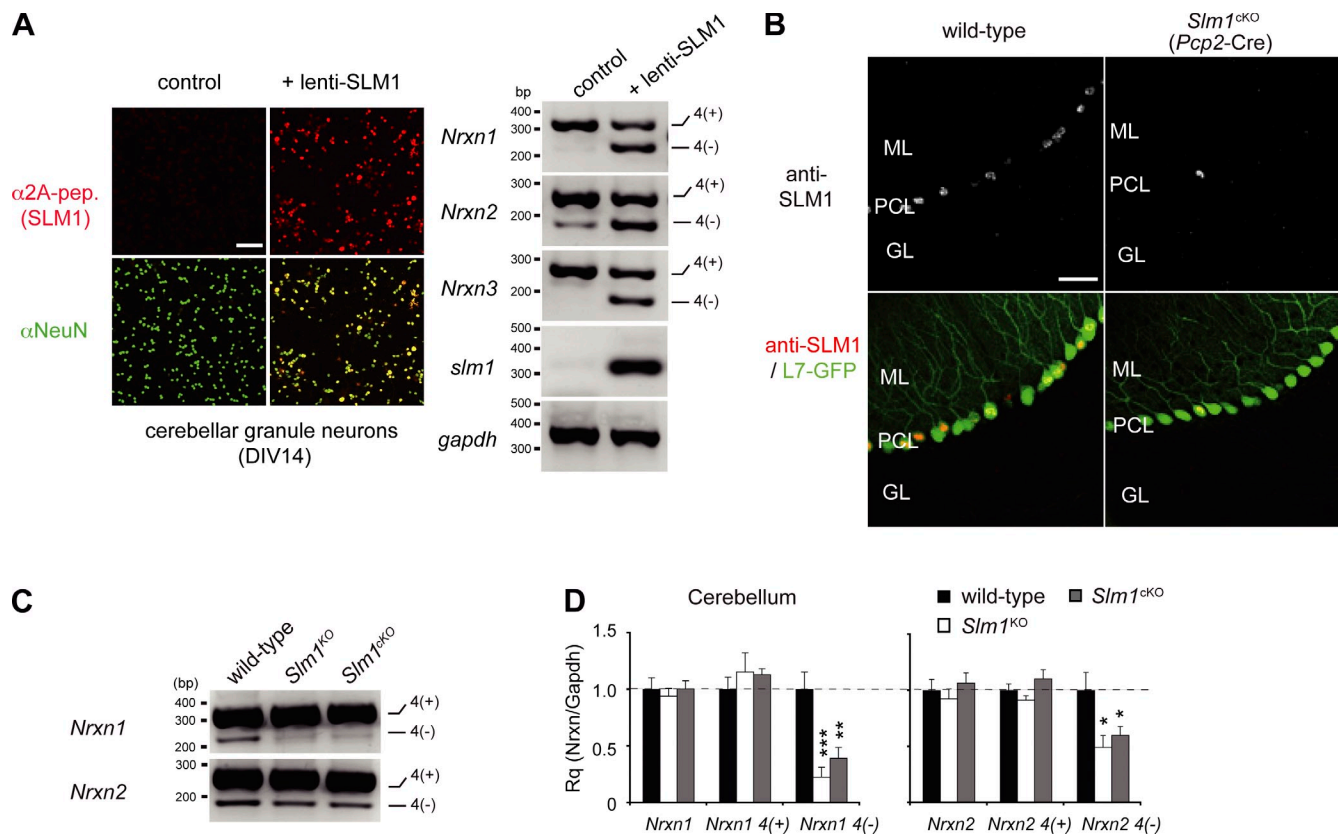


Figure 7. Cell type-specific alternative splicing of SLM1. (A) Shift in alternative splicing at *Nrxn1*, *Nrxn2*, and *Nrxn3* AS4 in cerebellar granule cells expressing SLM1 ectopically with lentiviral infection. Expression of 2A-tagged SLM1 in lentivirus-infected cerebellar granule cells was confirmed by immunostaining with anti-2A antibody. Representative images of semi-quantitative RT-PCR with *Nrxn* AS4 in granule neurons with or without ectopic SLM1 expression. (B) High magnification views of SLM1 immunoreactivity in Purkinje cell-specific *Slm1*^{KO} (*Slm1*^{cKO}) mice. Purkinje cells are marked by transgenic expression of EGFP from the Purkinje cell-specific L7 promoter. Bar, 50 μ m. (C) Representative images of semi-quantitative RT-PCR with *Nrxn* AS4 in cerebellum from wild-type, *Slm1*^{KO}, and *Slm1*^{cKO} mice. (D) Quantitative RT-PCR for *Nrxn1* and *Nrxn2* AS4 in wild-type, *Slm1*^{KO}, and *Slm1*^{cKO} mice ($n = 4$ animals per genotype).

in the activity of the cre driver (Saito et al., 2005). Importantly, analysis of cerebellar RNA from *Slm1*^{cKO} mice reveals a severe reduction in the *Nrxn1* AS4(–) mRNA, whereas total *Nrxn1* α mRNA levels are unchanged (Fig. 7, C and D). Thus, the vast majority of *Nrxn1* AS4(–) and *Nrxn2* AS4(–) isoforms in the cerebellum is derived from Purkinje cells where their expression depends on a cell-autonomous function of SLM1. Global ablation of SLM1 did not result in a significant further reduction of *Nrxn1* AS4(–) levels, consistent with the conclusion that SLM1 functions specifically in Purkinje cells. Similarly, *Nrxn2* AS4(–) was significantly reduced in *Slm1*^{cKO} and *Slm1*^{KO} mice (Fig. 7, C and D), further confirming a critical function of SLM1 in alternative splicing of *Nrxn2* mRNA in vivo.

Discussion

Previous work has led to the identification of several families of neuronal RNA-regulatory proteins, including neuro-oncological ventral antigen (Nova-1, -2), neural poly-pyrimidine tract binding protein (nPTBP), and ELAV family proteins (CELFs), which regulate alternative exons in neuronal tissues (Darnell, 2013; Kuroyanagi et al., 2013). These factors direct generation of neuron-specific splice variants that are absent from neuronal precursor

or nonneuronal cells. By contrast, RNA-binding proteins that drive the unique expression patterns of neuronal sub-populations, such as specific interneuron classes, are less well understood.

Role for SLM1 in the generation of neuron-specific molecular repertoires

In this study we demonstrate that ectopic expression of SLM1 in a neuronal population that normally is SLM1 deficient is sufficient to trigger production of specific neurexin splice variants. Moreover, conditional knock-out of SLM1 in an SLM1-positive specific cell type results in a severe loss of specific neurexin splice variants in the cerebellum in vivo. This cell type-specific ablation of SLM1 also provides evidence that the lost splice variants were indeed selectively expressed in the cerebellar Purkinje cells. Therefore, our results begin to unravel cell type-specific neurexin isoform repertoires in neuronal populations in vivo. In the hippocampus, SLM1 is highly expressed in SCA and PPA interneurons. This class of GABAergic cells innervates CA1 pyramidal cell dendrites in the S.R. and is subject to specific forms of neuromodulatory regulation (Lawrence, 2008; Klausberger, 2009). In analogy to our findings in cerebellar neurons, we propose that selective expression of SLM1 drives a corresponding program of cell type-specific alternative splicing events in the hippocampus.

Synergistic and differential functions of SAM68 and SLM proteins

In a previous study, we reported a dynamic regulation of *Nrxn1* AS4 by SAM68, a closely related alternative splicing factor (Iijima et al., 2011). However, expression and function of SAM68 and SLM1 differ in several fundamental aspects. SAM68 activity toward *Nrxn1* AS4 depends on activation through neuronal signaling. Thus, the presence of SAM68 in a cell population is not predictive of *Nrxn1* isoform choice (Iijima et al., 2011). Moreover, SAM68 is broadly expressed across neuronal and nonneuronal cells (Richard et al., 2005; Paronetto et al., 2009). By contrast, SLM1 exhibits a more restricted expression pattern. Our gain-of-function and loss-of-function studies demonstrate that SLM1 instructs cell type-specific alternative splicing choices. Moreover, our experiments uncover a complex interplay between SAM68 and SLM1 activities as the regulation of alternative splicing at AS4 differs significantly for *Nrxn1*, -2, and -3 transcripts. While SAM68 and SLM1 synergize in driving exon skipping at AS4 in *Nrxn1*, they antagonize each other at *Nrxn3* AS4 in vivo. We demonstrated that specific sequences in the RNA-binding domain of SLM1 are required for regulation of *Nrxn2* AS4, which is insensitive to SAM68. Finally, our in vitro experiments support a model where hetero-oligomerization of SAM68 with SLM1 provides one potential mechanism that gates substrate specificity of SLM1, and thereby a further mechanism for regulation. Interestingly, a recent study by Elliott and colleagues demonstrated a splicing regulatory function of SLM2 toward *Nrxn2* that is similar to the function for SLM1 described here. Based on a comparison of regional SLM2 expression and estimates of *Nrxn1* AS4(-) abundance they suggested that SLM2 is the primary regulator of *Nrxn1* AS4(-) in vivo (Ehrmann et al., 2013). Considering the largely nonoverlapping expression patterns of SLM1 and SLM2 across cell populations as well as our global and cell type-specific knockout analysis of SLM1, we conclude that SLM2 is not the sole regulator of *Nrxn1* AS4 in vivo. Instead, we demonstrate with gain-of-function and loss-of-function experiments that SLM1 as well as SAM68 have major, cell type-specific contributions to *Nrxn* alternative splice variant choices in vivo.

Functional relevance of SLM1 in the developing nervous system

Neuronal subtype-specific alternative splicing patterns might contribute to the unique functional properties of neuronal cell populations. Such a mechanism is particularly attractive for polymorphic receptor families such as the neuexins that may contribute to specific cellular interactions or specific synaptic functions (Missler and Südhof, 1998; Boucard et al., 2005; Chih et al., 2006; Graf et al., 2006; de Wit et al., 2009; Baudouin and Scheiffele, 2010; Futai et al., 2013). Further work will be needed to understand the respective contributions of SAM68 and SLM proteins in shaping cell type-specific neuexin isoform contents. Moreover, neuexins are likely to be only one of many targets for SLM-dependent alternative splicing regulation. Our analysis of *Sam68:Slm1^{DKO}* animals uncovered the presence of ectopic Purkinje cells and defects in the foliation of the cerebellar cortex. These two aspects of the phenotype are most likely

linked considering that Purkinje cell anchoring centers have been proposed to instruct the foliation process (Sudarov and Joyner, 2007). Specifically, we observed loss of the fissure between lobules VI and VII in the cerebellar vermis. Whereas the primary and secondary fissures flanking lobules VI–VIII form during late embryonic development, the separation of lobules VI and VII occurs during the first postnatal week (Altman and Bayer, 1997). The STAR protein pre-mRNA substrates relevant for this phenotype remain to be identified. Notably, similar foliation defects have been reported in knockout mice for several other neuronal signaling proteins (Sadakata et al., 2007; Lancaster et al., 2011). Definition of the complete alternative splicing programs for STAR proteins as well as the dissection of cellular phenotypes of SLM1-deficient neurons should provide important next steps in testing the links between cell type-specific alternative splicing programs and neuronal development.

Materials and methods

Antibodies and DNA constructs

Polyclonal antibodies to SAM68, SLM1, and SLM2 were raised in rabbits and guinea pigs using the following synthetic peptides (amino acids in brackets were added to improve solubility of the peptide and for coupling): RGVPPPTVRGAPTRAR-[C] (anti-SAM68), VNEDAYDSYAPEEWAT-[KKKC] (anti-SLM1), and PRARGVPPTGYRP-[C] (anti-SLM2; Iijima et al., 2011). Anti-GFP antibodies were raised in rabbits using recombinant GFP expressed in *Escherichia coli* as an antigen (Taniguchi et al., 2007). The following commercially available antibodies were used: mouse anti- β -tubulin (E7; DSHB), mouse anti-Fox3/NeuN (MAB377; EMD Millipore), rat anti-HA (clone 3F10; Roche), sheep anti-parvalbumin (R&D Systems), mouse anti-calbindin (Swant), goat anti-calretinin (Swant), rabbit anti-VIP (Immuno-star), mouse anti-cholecystokinin (CCK8; Abcam), goat anti-ROR α (C-16; Santa Cruz Biotechnology, Inc.), rabbit anti-vesicular glutamate transporter 1 (vGluT1, #1353303; Synaptic Systems), rabbit anti-vesicular glutamate transporter 2 (vGluT2, #135403; Synaptic Systems), guinea pig anti-vesicular GABA transporter (vGAT, #676780; EMD Millipore), and rabbit anti-2A peptide (EMD Millipore).

Somatostatin-positive interneurons were marked in Somatostatin-IRES-cre mice crossed to tdTomato reporter mice (Madisen et al., 2010; Taniguchi et al., 2011).

Expression vectors (pEGFP backbone, CMV promoter) for SAM68, SLM1, SLM2, hnRNPA1, hnRNPH, and *Nrxn1* AS4 splice reporters were described previously (Di Fruscio et al., 1999; Fiset et al., 2010; Iijima et al., 2011). The *Nrxn2* AS4 splice reporter contains a mouse *Nrxn2* genomic cassette of AS4 from exon 19 to exon 21 containing 500 bp intronic sequence at each splice donor and acceptor site.

RNA isolation and alternative splicing assays

Human embryonic kidney (HEK293 and HEK293T) cells were cultured in DMEM (Invitrogen) supplemented with 10% FCS, L-glutamine (2 mM), penicillin, and streptomycin and grown in 5% CO₂ at 37°C. For reporter assays, cells were cotransfected using Fugene 6 reagent (Roche) with expression vectors encoding the splice reporter and RNA-binding proteins. RNA was harvested 24–36 h after transfection using Trizol reagent (Invitrogen), followed by removal of contaminating DNA using Turbo DNA-free (RNase-free DNase; Ambion). 1 μ g of total RNA was reverse transcribed using random hexamers and ImProm-II (Promega).

For semi-quantitative PCR, DNA fragment intensities were quantified by image analyzer (FAS-III; Toyobo) and ImageGauge software (Fujifilm). Oligonucleotide primers used for semi-quantitative PCR were described previously (Iijima et al., 2011).

Quantitative PCR was performed on a StepOnePlus qPCR system (Applied Biosystems). Custom and commercial gene expression assays (see Table 1) were used with TaqMan Master Mix (Applied Biosystems) and comparative C_T method. The mRNA levels were normalized to that of *Gapdh* mRNA.

Biochemical procedures

Cells or brain tissues were lysed with RIPA buffer (25 mM Tris-HCl, pH 8.0, 150 mM NaCl, 1% NP-40, 1% deoxycholate, and 0.1% SDS) containing

Table 1. Oligonucleotide sequences of qPCR primer sets

Primer set	Catalogue number/sequence
<i>Nrxn1 alpha</i>	Mm00660298m1
<i>Nrxn2 alpha</i>	Mm01236851_m1
<i>Nrxn3 alpha</i>	Mm00553213_m1
<i>Gapdh</i>	Mm99999915g1
<i>Nrxn1 ex20F</i>	5'-TAGTTGATGAATGGCTACTCGACAAA-3'
<i>Nrxn1 ex20R</i>	5'-GACTCAGTTGTCATAGAGGAAGGCAC-3'
Probe	6FAM-CCGACCAGCCTCACATTCCCCACTAT-BBQ
<i>Nrxn1 delF</i>	5'-GCTACCCTGCAGGGCGT-3'
<i>Nrxn1 delR</i>	5'-GAGGTGGACATCTCAGACTGCAT-3'
Probe	6FAM-CCGACCAGCCTCACATTCCCCACTAT-BBQ
<i>Nrxn2 ex20F</i>	5'-GACATTACAATTGATGAGCCCAAC-3'
<i>Nrxn2 ex20R</i>	5'-CAGGCGCTCGTTATCAAAGTTT-3'
Probe	6FAM-CCATCGTGAGCGACGGCAAATATCAC-BBQ
<i>Nrxn2 delF</i>	5'-GACATTACAATTGATGAGCCCAAC-3'
<i>Nrxn2 delR</i>	5'-GTCAGCTGGCGTCCTGC-3'
Probe	6FAM-CCATCGTGAGCGACGGCAAATATCAC-BBQ
<i>Nrxn3 ex20F</i>	5'-AAATACCAGTTTGTGGCCTT-3'
<i>Nrxn3 ex20R</i>	5'-TTGGAGGCGTTTATTATCAGTGTT-3'
Probe	6FAM-CCATCGTGAGCGACGGCAAATATCAC-BBQ
<i>Nrxn3 delF</i>	5'-GAACTCCTGTCAATGATGGCAAATAC-3'
<i>Nrxn3 delR</i>	5'-TAGCTGCCGCGCTGTAGG-3'
Probe	6FAM-CCAGGAATGGGGAAATGTACTACT-BBQ

protease inhibitor cocktail (Roche). For protein interaction studies the soluble fractions were subjected to immunoprecipitation for 24 h at 4°C and analyzed by immunoblotting. For visualization, HRP-conjugated secondary antibody and enhanced chemiluminescence (ECL) detection (Thermo Fisher Scientific) were used. Signals were acquired using an image analyzer (LAS-3000; Fujifilm).

Immunohistochemistry, image acquisition, and analysis

Animals were transcardially perfused with fixative (4% paraformaldehyde/15% picric acid in 100 mM phosphate buffer, pH 7.2). Tissues were sectioned at 50 µm in PBS on a vibratome (VT1000S; Leica) and floating sections were immunostained following standard procedures (fluorophores Alexa Fluor 488, Alexa Fluor 568, Cy2, Cy3, Cy5, and mounting medium Fluoromount G). Images were acquired at room temperature on a confocal microscope (LSM5; Carl Zeiss) using 4x, 40x, and 63x Plan APOchromat objectives (NA 0.2, 1.3, and 1.4, respectively) and controlled by Zen 2008 software (Carl Zeiss). Images were assembled using Photoshop and Illustrator software (Adobe). For quantitative assessment of interneuron association of SLM proteins, coronal sections from three animals were prepared as described above and confocal images were captured on a confocal system (LSM5; Carl Zeiss) from 5–10 separate fields per animal from the dorsal hippocampal CA1–CA2 region. All procedures related to animal experimentation were reviewed and approved by the Kantonales Veterinäramt Basel-Stadt.

Production of lentivirus

VSV-G pseudotyped lentiviral vectors provided by St. Jude Children's Research Hospital (Memphis, TN; Hanawa et al., 2002) were used in this study. The pCL20c vectors were designed under the control of the MSCV promoter (Hawley et al., 1994). Viral supernatants were produced by cotransfection of HEK293T cells with a mixture of four plasmids using the calcium phosphate precipitation method. The four-plasmid mixture consisted of 6 µg of pCAG-kGP1R, 2 µg of pCAG-4RTR2, 2 µg of pCAG-VSV-G, and 10 µg of vector plasmid pCL20c MSCV-SLM1-2A-venus. Medium containing viral particles was harvested 40 h after transfection. The medium samples were filtered through 0.22-µm membranes and concentrated by centrifugation at 25,800 rpm for 90 min. The virus samples were suspended in cold PBS (pH 7.4), frozen in aliquots, and stored at –80°C.

Knockout mice

Sam68^{KO} mice were provided by S. Richard (McGill University, Montreal, Quebec, Canada; Richard et al., 2005). An *Slm1* conditional allele was generated by homologous recombination in mouse embryonic stem cells. In brief, a genomic DNA fragment containing exon 2 (ENSEMUSE00000314986) was flanked by a LoxP site and a FRT-PGK-neo-LoxP cassette encoding neomycin phosphotransferase under control of the phosphoglycerate kinase 1 promoter. The targeting vector was electroporated into 129SvEvTac embryonic stem cells. Homologous recombination in G-418-resistant clones was confirmed and selected cells were blastocyst injected. Chimeric animals were crossed with ROSA-26 Flpe mice to remove PGK-neo sequences through Frt/Flp-mediated excision. The *Slm1^{lox/+}* mice were crossed with *CMV^{cre}* deleter mice (Schwenk et al., 1995) to generate a germline deletion of *Khdrbs2*. Conditional ablation of *Khdrbs2* in Purkinje was done using *Pcp2^{cre}* knock-in mice (Saito et al., 2005). The *Slm1^{lox}* allele was detected by PCR using primers 5'-CCCTGAGAGGCTGAGGTTAG-3' (Lox gtf), 5'-AAGTGCAGTGCCACAAAATG-3' (Lox gtfR), 5'-CCACAAGCCATA-AAATTGAGC-3' (Frt gtf), and 5'-GCCAACACATTTGGCTAGAG-3' (Frt gtfR).

Sam68:Slm1^{DKO} mice were generated by intercrossing of the individual mutant mice. The resulting homozygous mutant mice were viable.

Statistical analysis

Pairwise comparisons were performed using Student's *t* test. For multiple comparisons, analysis of variance (ANOVA) followed by Bonferroni or Dunnett test was used. Data are represented as the mean ± SEM. Significance is indicated as follows: ***, *P* < 0.001; **, *P* < 0.01; *, *P* < 0.05.

Online supplemental material

Fig. S1 shows Western blot and immunohistochemical data on region-specific expression of SAM68 and SLM proteins. Fig. S2 shows high-resolution views of neuronal cell type-specific expression of SAM68 and SLM proteins in mouse hippocampus. Fig. S3 illustrates targeting strategy for generation of *Slm1^{KO}* mice and morphological analysis. Fig. S4 shows Purkinje cell-specific *Slm1^{KO}* mice. Online supplemental material is available at <http://www.jcb.org/cgi/content/full/jcb.201310136/DC1>.

We thank S. Baudouin and D. Schreiner for advice and comments on the manuscript, and S. Richard and N. Suzuki for generously sharing *Sam68^{KO}* and *Pcp2^{cre}* mice, respectively. We are grateful to E. Sylwestrak for generously sharing reagents, and C. Bornmann, L. Burklé, A. Yamaguchi, and Y. Doi for experimental support.

This work was supported by funds to P. Scheiffele from the Swiss National Science Foundation and the Kanton Basel-Stadt. T. Iijima was supported by the Uehara Memorial Foundation, KANAE Foundation for the Promotion of Medical Science, and Astellas Foundation for Research on Metabolic Disorders.

The authors declare no competing financial interests.

Submitted: 29 October 2013

Accepted: 23 December 2013

References

- Altman, J., and S.A. Bayer. 1997. Development of the cerebellar system: *In* Relation to Its Evolution, Structure, and Functions. CRC Press, Boca Raton, FL. 230–251.
- Aoto, J., D.C. Martinelli, R.C. Malenka, K. Tabuchi, and T.C. Südhof. 2013. Presynaptic neurexin-3 alternative splicing trans-synaptically controls postsynaptic AMPA receptor trafficking. *Cell*. 154:75–88. <http://dx.doi.org/10.1016/j.cell.2013.05.060>
- Baudouin, S., and P. Scheiffele. 2010. SnapShot: Neuroligin-neurexin complexes. *Cell*. 141:908.
- Beck, E.S., G. Gasque, W.L. Imlach, W. Jiao, B. Jiwon Choi, P.S. Wu, M.L. Kraushar, and B.D. McCabe. 2012. Regulation of Fasciclin II and synaptic terminal development by the splicing factor beag. *J. Neurosci.* 32:7058–7073. <http://dx.doi.org/10.1523/JNEUROSCI.3717-11.2012>
- Boucard, A.A., A.A. Chubykin, D. Comoletti, P. Taylor, and T.C. Südhof. 2005. A splice code for trans-synaptic cell adhesion mediated by binding of neuroligin 1 to alpha- and beta-neurexins. *Neuron*. 48:229–236. <http://dx.doi.org/10.1016/j.neuron.2005.08.026>
- Chih, B., L. Gollan, and P. Scheiffele. 2006. Alternative splicing controls selective trans-synaptic interactions of the neuroligin-neurexin complex. *Neuron*. 51:171–178. <http://dx.doi.org/10.1016/j.neuron.2006.06.005>
- Craig, A.M., and Y. Kang. 2007. Neurexin-neuroligin signaling in synapse development. *Curr. Opin. Neurobiol.* 17:43–52. <http://dx.doi.org/10.1016/j.conb.2007.01.011>

- Darnell, R.B. 2013. RNA protein interaction in neurons. *Annu. Rev. Neurosci.* 36:243–270. <http://dx.doi.org/10.1146/annurev-neuro-062912-114322>
- de Wit, J., E. Sylwestrak, M.L. O'Sullivan, S. Otto, K. Tiglio, J.N. Savas, J.R. Yates III, D. Comolletti, P. Taylor, and A. Ghosh. 2009. LRRTM2 interacts with Neurexin1 and regulates excitatory synapse formation. *Neuron.* 64:799–806. <http://dx.doi.org/10.1016/j.neuron.2009.12.019>
- Dean, C., F.G. Scholl, J. Choih, S. DeMaria, J. Berger, E. Isacoff, and P. Scheiffele. 2003. Neurexin mediates the assembly of presynaptic terminals. *Nat. Neurosci.* 6:708–716. <http://dx.doi.org/10.1038/nn1074>
- Di Fruscio, M., T. Chen, and S. Richard. 1999. Characterization of Sam68-like mammalian proteins SLM-1 and SLM-2: SLM-1 is a Src substrate during mitosis. *Proc. Natl. Acad. Sci. USA.* 96:2710–2715. <http://dx.doi.org/10.1073/pnas.96.6.2710>
- Ehrmann, I., C. Dalgliesh, Y. Liu, M. Danilenko, M. Crosier, L. Overman, H.M. Arthur, S. Lindsay, G.J. Clowry, J.P. Venables, et al. 2013. The tissue-specific RNA binding protein T-STAR controls regional splicing patterns of neurexin pre-mRNAs in the brain. *PLoS Genet.* 9:e1003474. <http://dx.doi.org/10.1371/journal.pgen.1003474>
- Fisette, J.F., J. Toutant, S. Dugré-Brisson, L. Desgroseillers, and B. Chabot. 2010. hnRNP A1 and hnRNP H can collaborate to modulate 5' splice site selection. *RNA.* 16:228–238. <http://dx.doi.org/10.1261/rna.1890310>
- Futai, K., C.D. Doty, B. Baek, J. Ryu, and M. Sheng. 2013. Specific trans-synaptic interaction with inhibitory interneuronal neurexin underlies differential ability of neuroligins to induce functional inhibitory synapses. *J. Neurosci.* 33:3612–3623. <http://dx.doi.org/10.1523/JNEUROSCI.1811-12.2013>
- Galarneau, A., and S. Richard. 2009. The STAR RNA binding proteins GLD-1, QKI, SAM68 and SLM-2 bind bipartite RNA motifs. *BMC Mol. Biol.* 10:47. <http://dx.doi.org/10.1186/1471-2199-10-47>
- Gehman, L.T., P. Meera, P. Stoilov, L. Shiu, J.E. O'Brien, M.H. Meisler, M. Ares Jr., T.S. Otis, and D.L. Black. 2012. The splicing regulator Rbfox2 is required for both cerebellar development and mature motor function. *Genes Dev.* 26:445–460. <http://dx.doi.org/10.1101/gad.182477.111>
- Graf, E.R., Y. Kang, A.M. Hauner, and A.M. Craig. 2006. Structure function and splice site analysis of the synaptogenic activity of the neurexin-1 beta LNS domain. *J. Neurosci.* 26:4256–4265. <http://dx.doi.org/10.1523/JNEUROSCI.1253-05.2006>
- Hanawa, H., P.F. Kelly, A.C. Nathwani, D.A. Persons, J.A. Vandergriff, P. Hargrove, E.F. Vanin, and A.W. Nienhuis. 2002. Comparison of various envelope proteins for their ability to pseudotype lentiviral vectors and transduce primitive hematopoietic cells from human blood. *Mol. Ther.* 5:242–251.
- Hawley, R.G., F.H. Lieu, A.Z. Fong, and T.S. Hawley. 1994. Versatile retroviral vectors for potential use in gene therapy. *Gene Ther.* 1:136–138.
- Iijima, T., K. Wu, H. Witte, Y. Hanno-Iijima, T. Glatter, S. Richard, and P. Scheiffele. 2011. SAM68 regulates neuronal activity-dependent alternative splicing of neurexin-1. *Cell.* 147:1601–1614. <http://dx.doi.org/10.1016/j.cell.2011.11.028>
- Klausberger, T. 2009. GABAergic interneurons targeting dendrites of pyramidal cells in the CA1 area of the hippocampus. *Eur. J. Neurosci.* 30:947–957. <http://dx.doi.org/10.1111/j.1460-9568.2009.06913.x>
- Klein, M.E., T.J. Younts, P.E. Castillo, and B.A. Jordan. 2013. RNA-binding protein Sam68 controls synapse number and local β -actin mRNA metabolism in dendrites. *Proc. Natl. Acad. Sci. USA.* 110:3125–3130. <http://dx.doi.org/10.1073/pnas.1209811110>
- Kuroyanagi, H., Y. Watanabe, and M. Hagiwara. 2013. CELF family RNA-binding protein UNC-75 regulates two sets of mutually exclusive exons of the unc-32 gene in neuron-specific manners in *Caenorhabditis elegans*. *PLoS Genet.* 9:e1003337. <http://dx.doi.org/10.1371/journal.pgen.1003337>
- Lancaster, M.A., D.J. Gopal, J. Kim, S.N. Saleem, J.L. Silhavy, C.M. Louie, B.E. Thacker, Y. Williams, M.S. Zaki, and J.G. Gleeson. 2011. Defective Wnt-dependent cerebellar midline fusion in a mouse model of Joubert syndrome. *Nat. Med.* 17:726–731. <http://dx.doi.org/10.1038/nm.2380>
- Lawrence, J.J. 2008. Cholinergic control of GABA release: emerging parallels between neocortex and hippocampus. *Trends Neurosci.* 31:317–327. <http://dx.doi.org/10.1016/j.tins.2008.03.008>
- Lipscombe, D., A. Andrade, and S.E. Allen. 2013. Alternative splicing: functional diversity among voltage-gated calcium channels and behavioral consequences. *Biochim. Biophys. Acta.* 1828:1522–1529. <http://dx.doi.org/10.1016/j.bbame.2012.09.018>
- Madisen, L., T.A. Zwingman, S.M. Sunkin, S.W. Oh, H.A. Zariwala, H. Gu, L.L. Ng, R.D. Palmier, M.J. Hawrylycz, A.R. Jones, et al. 2010. A robust and high-throughput Cre reporting and characterization system for the whole mouse brain. *Nat. Neurosci.* 13:133–140. <http://dx.doi.org/10.1038/nm.2467>
- Masland, R.H. 2004. Neuronal cell types. *Curr. Biol.* 14:R497–R500. <http://dx.doi.org/10.1016/j.cub.2004.06.035>
- Matsuda, K., and M. Yuzaki. 2011. Cbln family proteins promote synapse formation by regulating distinct neurexin signaling pathways in various brain regions. *Eur. J. Neurosci.* 33:1447–1461. <http://dx.doi.org/10.1111/j.1460-9568.2011.07638.x>
- Meyer, N.H., K. Tripsianes, M. Vincendeau, T. Madl, F. Kateb, R. Brack-Werner, and M. Sattler. 2010. Structural basis for homodimerization of the Src-associated during mitosis, 68-kDa protein (Sam68) Qual domain. *J. Biol. Chem.* 285:28893–28901. <http://dx.doi.org/10.1074/jbc.M110.126185>
- Missler, M., and T.C. Südhof. 1998. Neurexins: three genes and 1001 products. *Trends Genet.* 14:20–26. [http://dx.doi.org/10.1016/S0168-9525\(97\)01324-3](http://dx.doi.org/10.1016/S0168-9525(97)01324-3)
- Okaty, B.W., K. Sugino, and S.B. Nelson. 2011. Cell type-specific transcriptomics in the brain. *J. Neurosci.* 31:6939–6943. <http://dx.doi.org/10.1523/JNEUROSCI.0626-11.2011>
- Paronetto, M.P., V. Messina, E. Bianchi, M. Barchi, G. Vogel, C. Moretti, F. Palombi, M. Stefanini, R. Geremia, S. Richard, and C. Sette. 2009. Sam68 regulates translation of target mRNAs in male germ cells, necessary for mouse spermatogenesis. *J. Cell Biol.* 185:235–249. <http://dx.doi.org/10.1083/jcb.200811138>
- Rajan, P., C. Dalgliesh, C.F. Bourgeois, M. Heiner, K. Emami, E.L. Clark, A. Bindereif, J. Stevenin, C.N. Robson, H.Y. Leung, and D.J. Elliott. 2009. Proteomic identification of heterogeneous nuclear ribonucleoprotein L as a novel component of SLM/Sam68 Nuclear Bodies. *BMC Cell Biol.* 10:82. <http://dx.doi.org/10.1186/1471-2121-10-82>
- Richard, S., N. Torabi, G.V. Franco, G.A. Tremblay, T. Chen, G. Vogel, M. Morel, P. Cléroux, A. Forget-Richard, S. Komarova, et al. 2005. Ablation of the Sam68 RNA binding protein protects mice from age-related bone loss. *PLoS Genet.* 1:e74. <http://dx.doi.org/10.1371/journal.pgen.0010074>
- Sadakata, T., W. Kakegawa, A. Mizoguchi, M. Washida, R. Katoh-Semba, F. Shutoh, T. Okamoto, H. Nakashima, K. Kimura, M. Tanaka, et al. 2007. Impaired cerebellar development and function in mice lacking CAPS2, a protein involved in neurotrophin release. *J. Neurosci.* 27:2472–2482. <http://dx.doi.org/10.1523/JNEUROSCI.2279-06.2007>
- Saito, H., H. Tsumura, S. Otake, A. Nishida, T. Furukawa, and N. Suzuki. 2005. L7/PCP-2-specific expression of Cre recombinase using knock-in approach. *Biochem. Biophys. Res. Commun.* 331:1216–1221. <http://dx.doi.org/10.1016/j.bbrc.2005.04.043>
- Schwenk, F., U. Baron, and K. Rajewsky. 1995. A cre-transgenic mouse strain for the ubiquitous deletion of loxP-flanked gene segments including deletion in germ cells. *Nucleic Acids Res.* 23:5080–5081. <http://dx.doi.org/10.1093/nar/23.24.5080>
- Shen, K., and P. Scheiffele. 2010. Genetics and cell biology of building specific synaptic connectivity. *Annu. Rev. Neurosci.* 33:473–507. <http://dx.doi.org/10.1146/annurev-neuro.051508.135302>
- Siddiqui, T.J., R. Pancaroglu, Y. Kang, A. Rooyackers, and A.M. Craig. 2010. LRRTMs and neuroligins bind neurexins with a differential code to cooperate in glutamate synapse development. *J. Neurosci.* 30:7495–7506. <http://dx.doi.org/10.1523/JNEUROSCI.0470-10.2010>
- Stoss, O., T. Novoyatleva, M. Gencheva, M. Olbrich, N. Benderska, and S. Stamm. 2004. p59(fyn)-mediated phosphorylation regulates the activity of the tissue-specific splicing factor rSLM-1. *Mol. Cell. Neurosci.* 27:8–21. <http://dx.doi.org/10.1016/j.mcn.2004.04.011>
- Sudarav, A., and A.L. Joyner. 2007. Cerebellum morphogenesis: the foliation pattern is orchestrated by multi-cellular anchoring centers. *Neural Dev.* 2:26. <http://dx.doi.org/10.1186/1749-8104-2-26>
- Südhof, T.C. 2008. Neuroligins and neurexins link synaptic function to cognitive disease. *Nature.* 455:903–911. <http://dx.doi.org/10.1038/nature07456>
- Taniguchi, H., L. Gollan, F.G. Scholl, V. Mahadomrongkul, E. Dobler, N. Limthong, M. Peck, C. Aoki, and P. Scheiffele. 2007. Silencing of neuroligin function by postsynaptic neurexins. *J. Neurosci.* 27:2815–2824. <http://dx.doi.org/10.1523/JNEUROSCI.0032-07.2007>
- Taniguchi, H., M. He, P. Wu, S. Kim, R. Paik, K. Sugino, D. Kvitsiani, Y. Fu, J. Lu, Y. Lin, et al. 2011. A resource of Cre driver lines for genetic targeting of GABAergic neurons in cerebellar cortex. *Neuron.* 71:995–1013. <http://dx.doi.org/10.1016/j.neuron.2011.07.026>
- Uemura, T., S.J. Lee, M. Yasumura, T. Takeuchi, T. Yoshida, M. Ra, R. Taguchi, K. Sakimura, and M. Mishina. 2010. Trans-synaptic interaction of GluDelta2 and Neurexin through Cbln1 mediates synapse formation in the cerebellum. *Cell.* 141:1068–1079. <http://dx.doi.org/10.1016/j.cell.2010.04.035>
- Venables, J.P., C. Vernet, S.L. Chew, D.J. Elliott, R.B. Cowmeadow, J. Wu, H.J. Cooke, K. Artzt, and I.C. Eperon. 1999. T-STAR/ETOILE: a novel relative of SAM68 that interacts with an RNA-binding protein implicated in spermatogenesis. *Hum. Mol. Genet.* 8:959–969. <http://dx.doi.org/10.1093/hmg/8.6.959>
- Zheng, S., and D.L. Black. 2013. Alternative pre-mRNA splicing in neurons: growing up and extending its reach. *Trends Genet.* 29:442–448. <http://dx.doi.org/10.1016/j.tig.2013.04.003>
- Zipursky, S.L., and J.R. Sanes. 2010. Chemoaffinity revisited: dscams, protocadherins, and neural circuit assembly. *Cell.* 143:343–353. <http://dx.doi.org/10.1016/j.cell.2010.10.009>

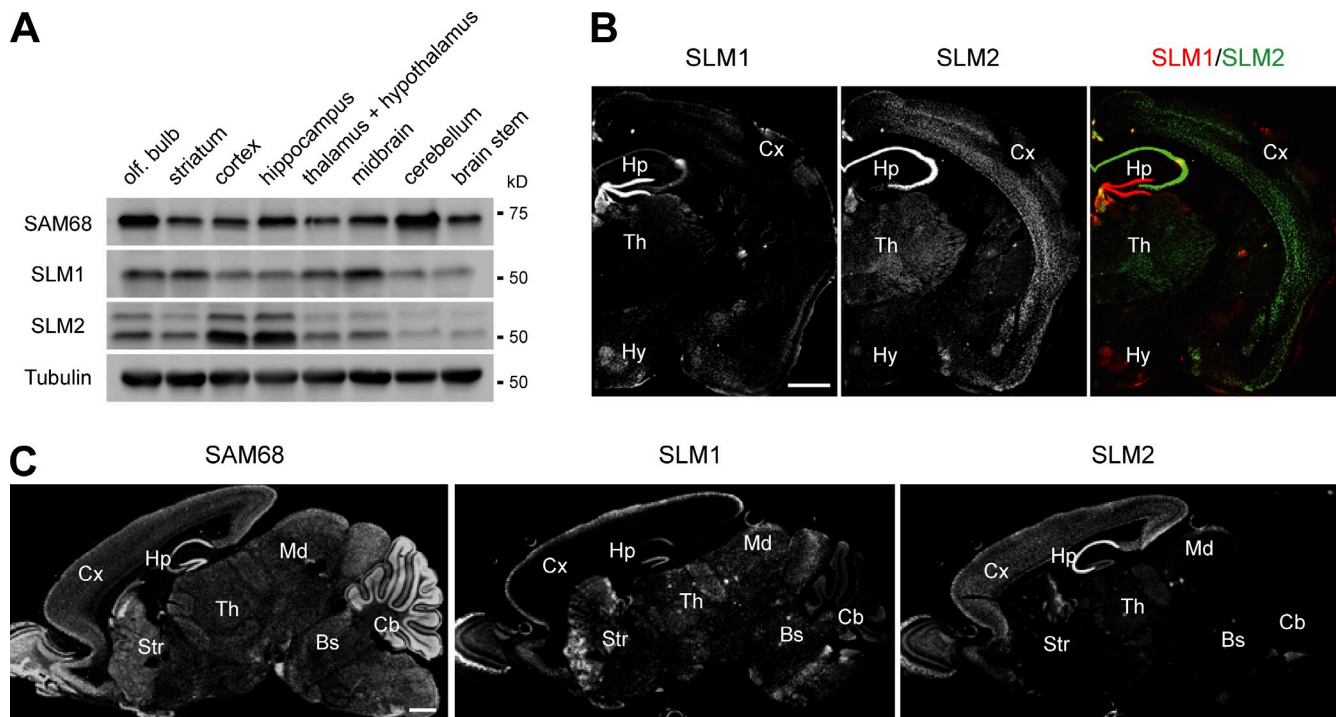
Iijima et al., <http://www.jcb.org/cgi/content/full/jcb.201310136/DC1>

Figure S1. **Region-specific expression of SAM68 and SAM68-like mammalian proteins in mouse brain.** (A) Western blot analysis of SAM68, SLM1, and SLM2 protein expression across mouse brain regions with isoform-specific antibodies. (B) Immunohistochemical detection of SLM1 and SLM2 with isoform-specific antibodies in coronal sections of adult mouse brain. A rostral section across cortex (Cx), hippocampus (Hp), thalamus (Th), and hypothalamus (Hy) is shown. Bar, 1 mm. (C) Immunohistochemical detection of SAM68, SLM1, and SLM2 with isoform-specific antibodies in the developing mouse brain (post-natal day 8; Str, striatum; Bs, brainstem; Md, midbrain; Cb, cerebellum). Bar, 1 mm.

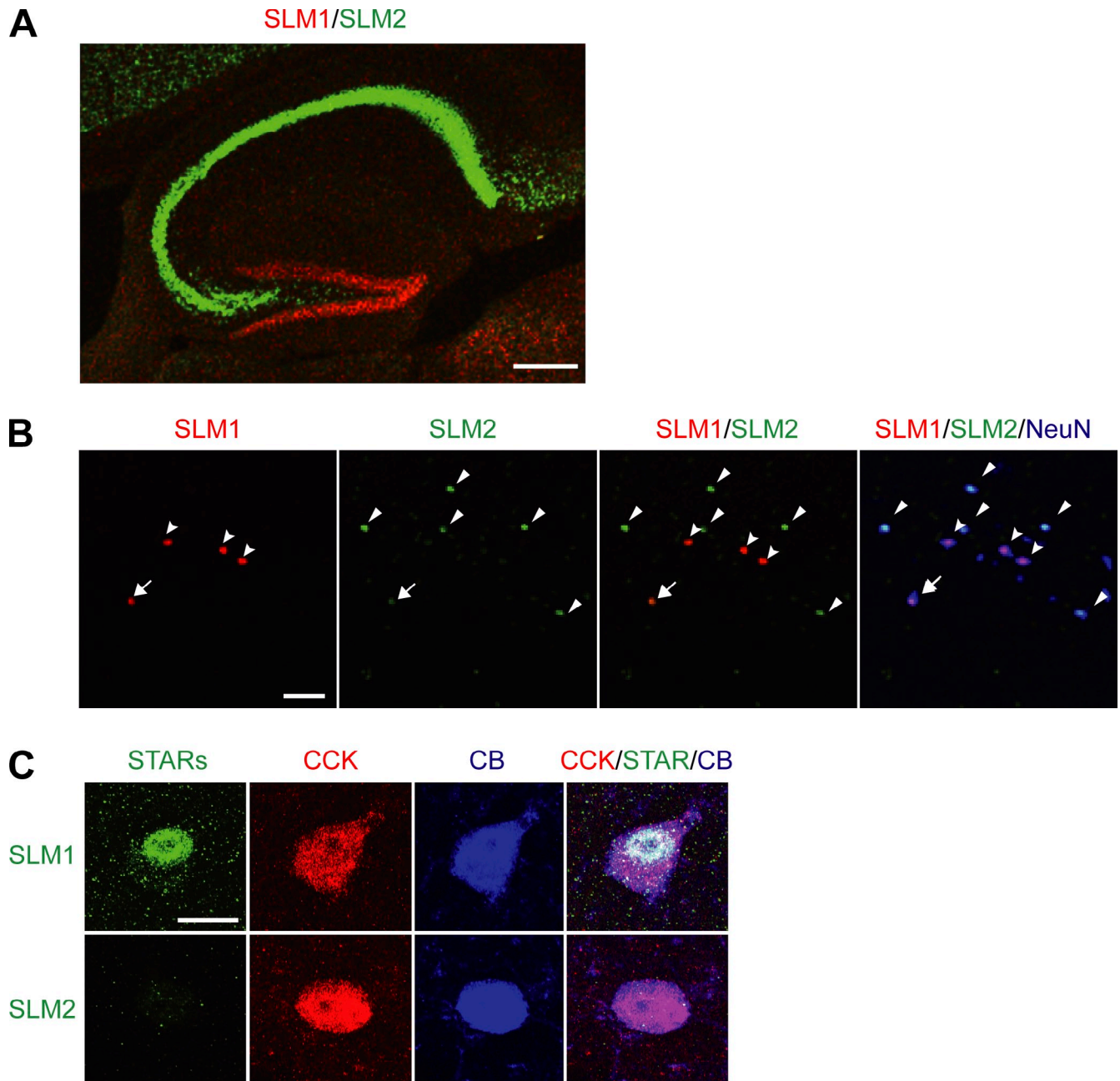


Figure S2. **Neuronal cell type-specific expression of SAM68 and SAM68-like mammalian proteins in mouse hippocampus.** (A) Co-immunohistostaining with anti-SLM1 (red) and SLM2 (green) antibodies in mouse hippocampal regions. Bar, 1 mm. (B) SLM1 (red) and SLM2 (green) are expressed in different interneuron populations in striatum radiatum. Interneurons were detected by co-immunostaining with anti-NeuN (blue). Bar, 50 μ m. (C) Triple staining of anti-SLM antibodies (red) with interneuron markers anti-calbindin antibody (blue) and anti-cholecystokinin antibody (red). SLM1 was highly expressed in the calbindin/cholecystokinin double-positive interneurons. Bar, 10 μ m.

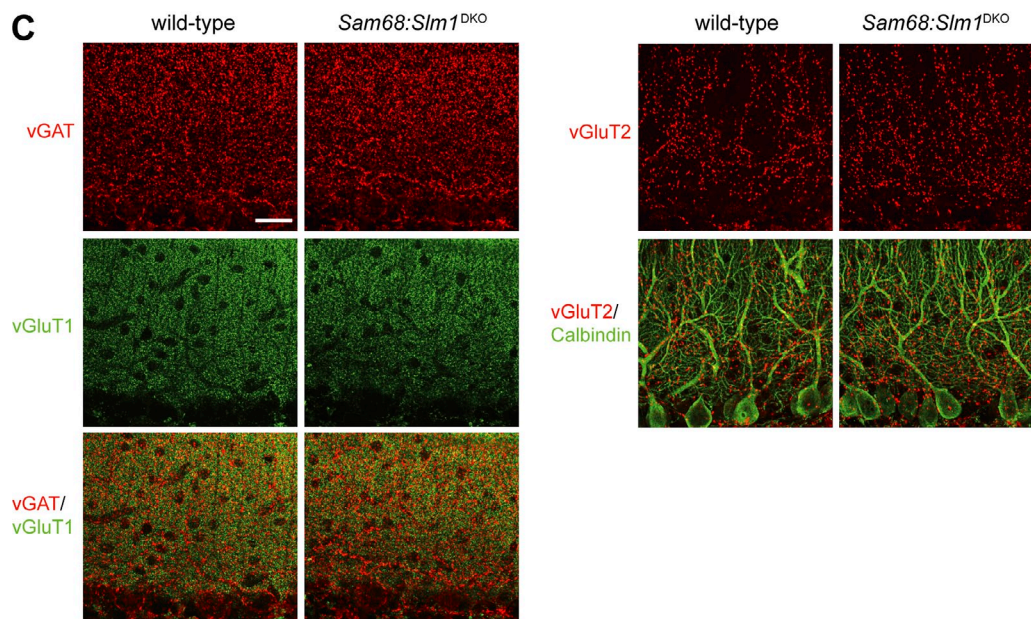
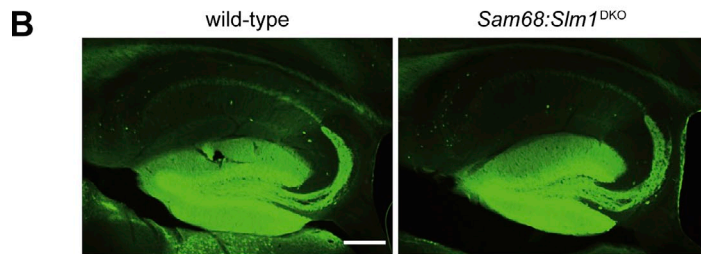
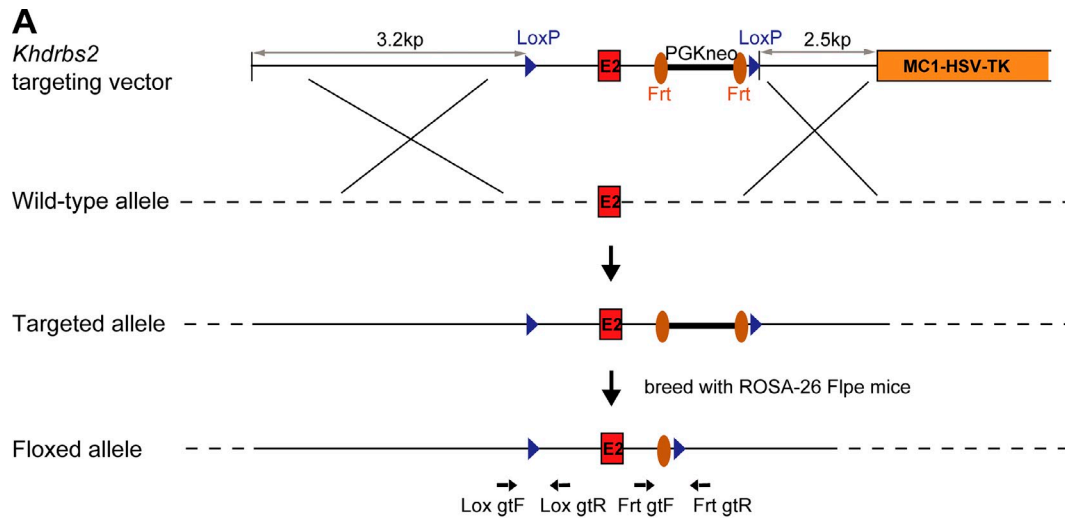


Figure S3. **Generation of *Slm1^{KO}* mice.** (A) Targeting strategy for conditional ablation of *Slm1* in mice. The *Khdrbs2* gene encoding SLM1 was modified by insertion of loxP sites flanking exon 2 (blue) and targeted ES cells isolated based on G418 resistance conferred by the PGKneo cassette. PGKneo was subsequently excised by breeding to ROSA-26 Flpe mice. The translational start codon is encoded in exon 1, after removal of exon 2, splicing into exon 3 results in a shift in translational reading frame. The RNA-binding KH domain of SLM1 is encoded in exons 3, 4, and 5. (B) Normal morphology of dentate gyrus region in the hippocampus of *Sam68/Slm1^{DKO}* cerebellum. Overall morphology of granule cells in dentate gyrus was visualized by immunostaining with anti-calbindin antibody. Bar, 1 mm. (C) Normal synaptic inputs into Purkinje cells in *Sam68/Slm1^{DKO}* cerebellum. Synapses from parallel fibers are detected by vGluT1, a marker for excitatory presynapses. Synapses from climbing fibers are detected by vGluT2, a marker for excitatory presynapses. Synapses from interneurons in molecular layer are detected by vGAT, a marker for inhibitory presynapses. Purkinje cells were marked by anti-calbindin antibody. Bar, 50 μ m.

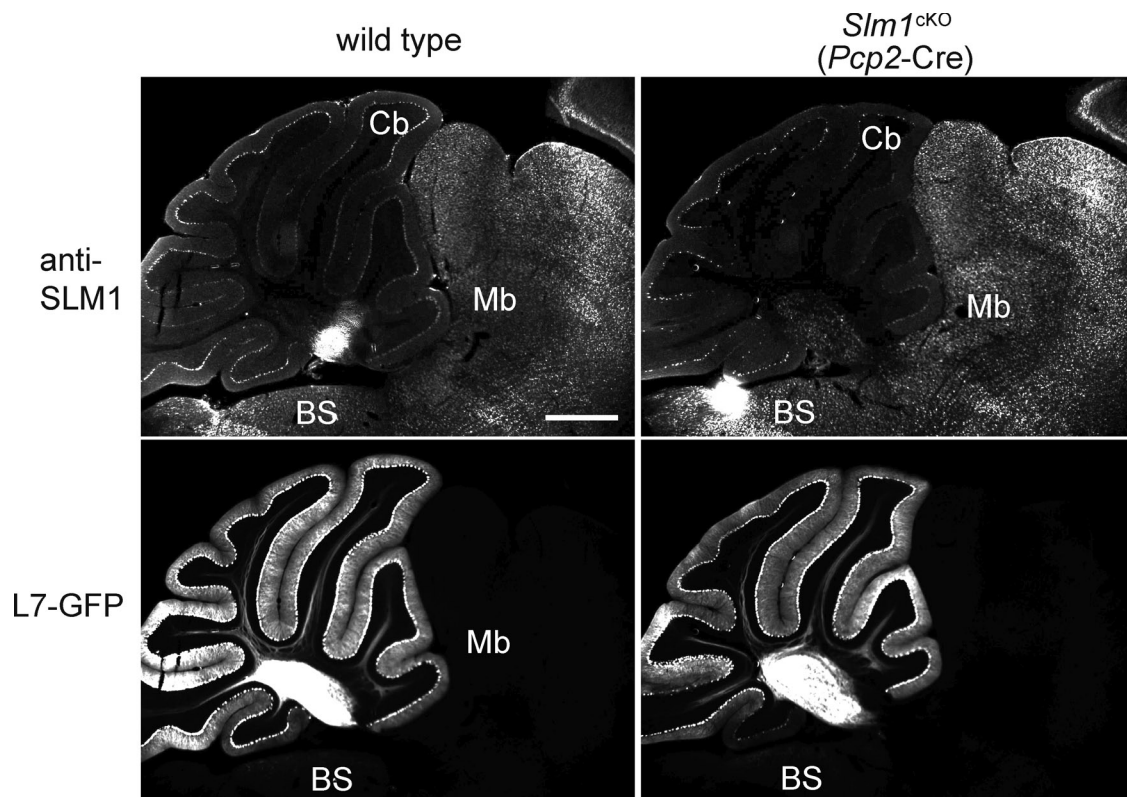


Figure S4. **Generation of Purkinje cell-specific *Slm1* knockout (*Slm1*^{ckO}) mice.** Low views of para-sagittal sections of cerebellum demonstrates anti-SLM1 immunoreactivity in cerebellar Purkinje cells, which is specifically lost in *Slm1*^{ckO}. Purkinje cells are marked by transgenic expression of EGFP from the Purkinje cell-specific L7-promoter. Bar, 1 mm.